Electronic Structures and Hydrogen Bond Network of High-Density and Very High-Density Amorphous Ices

ARTICLE *in* THE JOURNAL OF PHYSICAL CHEMISTRY B · NOVEMBER 2005

Impact Factor: 3.3 · DOI: 10.1021/jp0531558 · Source: PubMed

3 AUTHORS, INCLUDING:

C. He
Xi'an Jiaotong University
16 PUBLICATIONS **102** CITATIONS
SEE PROFILE

Qing Jiang
Jilin University
500 PUBLICATIONS **8,503** CITATIONS
SEE PROFILE

Electronic Structures and Hydrogen Bond Network of High-Density and Very High-Density Amorphous Ices

C. He, J. S. Lian, and Q. Jiang*

Key Laboratory of Automobile Materials, Ministry of Education, and Department of Materials Science and Engineering, Jilin University, Changchun 130025, China

Received: June 11, 2005; In Final Form: August 26, 2005

Electronic structures of hexagonal ice (ice I*h*), high-density amorphous ice (HDA), and very high-density amorphous ice (VHDA) are investigated using ab initio density functional theory (DFT) at 77 K under a pressure of 0.1 MPa, focusing on band structure, density of states (DOS), partial density of states (PDOS), and electron density. It is found that the integration intensity of the O-2p bonding band in HDA is 1.53 eV wider than that in the VHDA. Because more 2p electrons in HDA participate the 2p−1s hybridization of O−H. The classical molecular dynamics (MD) method has further been carried out to analyze the hydrogen bond network of HDA and VHDA with larger numbers of water molecules under the same temperature, pressure, and boundary conditions used as those during the DFT calculation. MD results show that there exists some water molecules with five hydrogen bonds in both HDA ($4.1 \pm 0.1\%$) and VHDA ($2.8 \pm 0.1\%$), as compared with the LDA, being consistent with the integration intensity results of PDOS. This result can be used to interpret the physical nature of the similar transition temperature of HDA and VHDA to LDA with different heating rates.

Introduction

Ice has not only 13 crystalline structures but also many types of amorphous structures, such as LDA, HDA, and VHDA.[1−5] HDA has been considered to be a glassy state of high-pressure liquid water[6−10] or a collapsed poorly crystalline phase of the ice I*h*,[10−13] and VHDA is considered a better candidate for the glassy phase continuous with the supercooled water. However, information of their electrical structures is little, which is important for understanding hydrogen bonding networks and for its effect on the electrochemical property of amorphous ices.

The similarity of structures between liquid water and HDA is shown by the existence of a so-called nonbonded interstitial molecule close to the first coordination shell of water molecules in both structures,[11] which is absent in LDA and ice I*h* but is reminiscent of the four nonbonded first neighbor molecules found in ice VII.[14] Finney et al. have deduced that "the coordination number (CN) = 5.0(0.1) of HDA signifies that five water molecules are present in the first neighbor shell. It means that the average each first neighbor shell has one interstitial molecule, while approximately two interstitial molecules are associated with VHDA as compared to the one in HDA. And these interstitial molecules act as lynch pins that keep HDA and VHDA structures intact. HDA−LDA and VHDA−LDA transitions cannot occur at low temperatures because the molecular kinetic energy is insufficient to let the interstitial molecules jump out of their first shell positions".[15,16] According to the previous illustration, HDA and VHDA have different structures and should have different HDA−LDA and VHDA−LDA transition temperatures. However, VHDA and HDA transform to LDA at the same temperature of 127 K at ambient pressure but with different heating rates.[16−18] Thus, a question is elicited as to whether the chemical bonding in HDA and VHDA is also different or whether the interstitial molecules of HDA and VHDA are hydrogen bonded to the central water molecule or not.

Computer simulations can simulate not only experiments with shorter time scales but also experiments that are difficult to realize. In addition, they can provide detailed structural information that is difficult to extract from experimental data. These advantages result in a large amount of simulation works to be carried out. The utility of the simulations for water is also confirmed by the fact that known structures of water have been reproduced.[19−27]

In this paper, through simulating structures of amorphous ices by DFT and classical MD methods, some interstitial molecules, which are hydrogen bonded to the central water molecules, are found. This kind of special bonding of interstitial molecules is about $4.1 \pm 0.1\%$ in HDA but $2.8 \pm 0.1\%$ in VHDA, which leads to similar energetic levels and transition temperatures of HDA−LDA and VHDA−LDA. In addition, our calculating method for electron density of amorphous ices supplies a way to predict the possible existence of hydrogen bonds in amorphous ices.

Simulation Details

Simulations are performed by the CASTEP software package[28] based on DFT in local density approximation through the Material Studio user interface. We used a plane wave basis set for the expansion of the wave functions where the electron−ion interaction was described by an ultrasoft pseudopotential, which is as soft as possible within the core region. Thus, the cutoff energy is dramatically reduced. With a cutoff energy of 380 eV and the *k*-points of $3 \times 3 \times 2$, sufficient numbers of wave functions are included so as to obtain precise information about the electronic structure of the ices. Calculations started with a *P*63/*mmc* space group. The structure of ice I*h* is

* To whom all correspondence should be addressed. E-mail: jiangq@jlu.edu.cn; fax: +86-431-5095876.

10.1021/jp0531558 CCC: $30.25
Published on Web 10/05/2005

composed of 32 molecules consisting of six ice I*h* unit cells that directly are shown by the Material Studio software package as a superlattice. The Langevin thermostat, which generates stochastic dynamics via a Brownian motion model, is implemented using the fluctuation−dissipation theorem where the decay rate of fluctuations is controlled by the damping time parameter to avoid a larger time scale of any motions of interest.

In the molecular dynamics simulations, we perform a *NPT* ensemble and choose to acquire HDA by pressurizing ice I*h* to a pressure $P = 1.2$ GPa at 77 K. After that, HDA is cooled to 77 K and decompressed as well.[6,7] The time step is 1 fs, and each process has simulation steps of 500−2000. ρ, the density of simulated HDA ($\rho = 1.17$ g/mL at $T = 77$ K under $P = 0.1$ MPa), is in excellent agreement with experimental results.[6,7] VHDA is formed by gradually densifying HDA further on heating at a constant $P = 1.1$ GPa up to $T = 165$ K. The obtained substance is cooled to 77 K and decompressed as well. The other parameters used are the same as that for HDA. The obtained ρ value of 1.24 g/mL at $T = 77$ K under $P = 0.1$ MPa for VHDA corresponds to experimental results.[29]

To obtain a more distinct hydrogen bond network, classical MD simulations were made by equilibrating a larger system at the same ρ and T of the smaller one. Then, the resulting configuration was used as a starting point of Dmol3 (based on DFT) for electron density analysis.

Classical *NPT* MD calculations have been performed under $P = 0-1.5$ GPa with a periodic boundary condition for hexagonal supercells containing 864 water molecules where the Parrinello−Rahman barostat[30] and the Berendsen thermostat[31] are used with a time step of 1 fs. Simulation times at each process are in the range of 50−200 ps. Electrostatic interactions are treated by the particle-mesh Ewald method.[32] To make sure of our result, hydrogen isotope substitution in the molecular dynamics simulations was used. The COMPASS (condensed-phase optimized molecular potentials for atomistic simulation studies) force field based on the earlier class II CFF9x and PCFF force fields has been adopted, which is the first ab initio base force field and has been parametrized using extensive data for molecules in the condensed phase. We used the reflex powder diffraction simulation method to simulate X-ray diffraction where the pseudo-Voige function was used. HDA and VHDA with isotope substitution D_2O recovered after compression under $P = 0.1$ MPa with liquid N_2 were characterized by X-ray simulation diffraction (Cu Kα, $\lambda = 1.540562$ Å). The corresponding diffractogram is shown in Figure 1a and is in agreement with the literature values where the maximum of the intense broad peak is at 3.0 Å.[6−7,33] The diffractogram of VHDA formed from HDA is further present in Figure 1b. The main diffraction peak of VHDA in comparison with that of HDA is sharpened, which is characterized by the decrease of the full width at half-height (fwhh) and by the shift from 3.0 Å to a higher scattering vector of 2.88 Å. These are in good agreement with experimental data.[29,34] All of the previous results confirm that our simulations have enough reliability and accuracy to study structures of amorphous ices.

Results and Discussion

The band structure, DOS and PDOS of ice I*h*, HDA, and VHDA calculated are shown in the Figure 2, where the band structures exhibit a typical insulating characteristic with distinct band gaps of 1.978 eV for ice I*h* (not shown), 4.810 eV for HDA, and 5.020 eV for VHDA. The band from −7 to 0 eV in HDA is continuous, while a band gap between −5.5 and −5.0 eV in VHDA is present, which denotes a distinct difference in the band structures between HDA and VHDA.

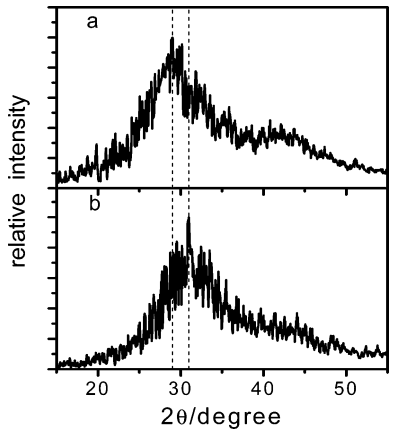

Figure 1. X-ray diffraction patterns of (a) HDA with isotope substitution (D_2O) made by compression of ice I*h* at 77 K and 1.2 GPa recovered at 77 K and 0.1 MPa and (b) VHDA with isotope substitution (D_2O) made by heating HDA under $P = 1.1$ GPa up to 165 K recovered at 77 K and 0.1 MPa.

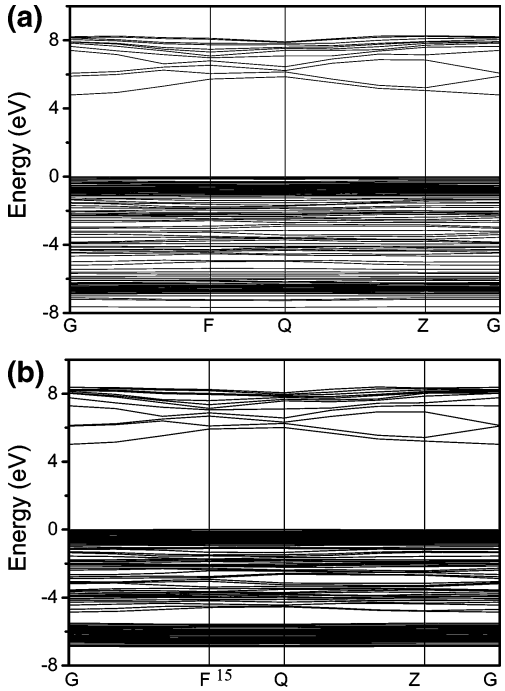

Figure 2. Band structures of (a) HDA and (b) VHDA.

The total DOS and PDOS of O-2p and H-1s electrons N(ϵ), calculated for ice I*h*, HDA, and VHDA, are shown in Figure 3. DOS near the Fermi level comes mainly from p electrons in the O ion and partially from s electrons in the H ion. We do not chart O-1s as it shows a very small effect on the total DOS in comparison with O-2p. For HDA and VHDA, the results show that the lowest band at about −18.5 eV is due to almost exclusive O-2s electrons, with a little degree of hybridized H-1s states. The next fully occupied sets of bands with higher energies consist of the overlapping bands of both the O-2p and the H-1s states, indicating a strong interaction between them. These bands represent the main covalent bonding component, exhibiting strong mixing. As for DOS, there is higher electric density in both HDA and VHDA than in ice I*h* near the Fermi level, while the corresponding difference between HDA and VHDA is little.

PDOS exhibits the integral intensity in HDA and VHDA for different bands. The valence state of O in both HDA and VHDA can be obtained via distribution of O-2p electrons in the t_{2g} and e_g^b bands where t_{2g} denotes the band from −1.5 to 0.9 eV, which

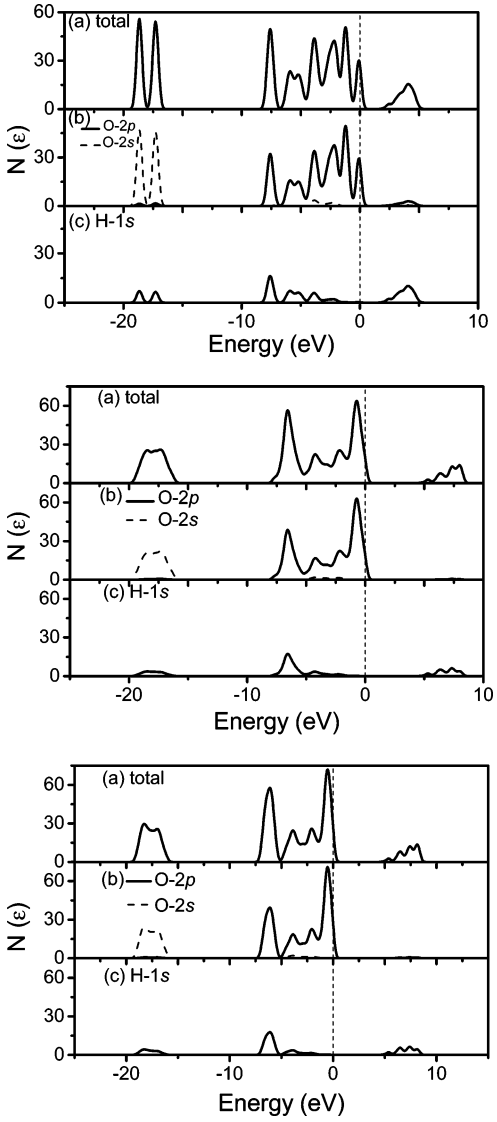

Figure 3. DOS and PDOS of ice I*h* (top), HDA (middle), and VHDA (bottom) where the parts (a−c) of the figures refer to DOS, PDOS (O), and PDOS (H), respectively.

TABLE 1: Integration Intensities of O-2*p* Bands in HDA and VHDA

	e_g*	t_{2g}	e_g[a]	total
O[b]	1.13406	66.07745	95.37573	162.58724
O[a]	1.29791	68.01572	93.84975	163.16338

[a] O in VHDA. [b] O in HDA.

points away from the hydrogen and to form nonbonding band, and e_g[b] shows the band from −8 to −1.5 eV, which is occupied by the p_x, p_y, and p_z orbitals directly overlapping with s orbital of the hydrogen along the tetrahedron directions. Integration of each band of O-2p PDOS is listed in Table 1. The antibonding band e_g* consisting of the states from 4 to 9 eV is also included. The total density does not change within the precision of the calculation. The integral intensity of PDOS of e_g[b] in HDA is 1.53 eV lower than that in VHDA, or the participating of 2p electrons in the 2p-1s hybridization of O−H of VHDA is less than those in HDA. Because this hybridization consists of covalent bonds and hydrogen bonds, there are more hydrogen bonds in HDA than in VHDA, while their covalence bond structures are the same according to results reported by Finney et al.[15,16] and our RDFs simulations. Correspondingly, an increase of 1.94 eV in the integral intensity of PDOS of t_{2g} in VHDA implies that the electrons of VHDA are more localized.

The simulations indicate that CN of O−H in both HDA and VHDA is about 2.1(0.1), which is more than two. Thus, some of these additional close water molecules should be hydrogen bonded to the central water molecule. To quantify the number of hydrogen bonds presented in water, a purely geometric definition is adopted: a hydrogen bond is identified when the distance between the hydrogen atom and the acceptor is less than or equal to 2.5 Å and when a hydrogen atom is located between two oxygen ions, such that −OHO is larger than 140°. The O ion may act as a hydrogen bond acceptor when it has at least one lone electron pair. Although somewhat arbitrary, this definition enables the identification of trends between different simulation conditions. On the basis of this definition, some five hydrogen bonded water molecules in both HDA and VHDA, but not in LDA, are found. The percentage of these interstitial molecules hydrogen bonded to the central water molecules is about 2.8 ± 0.1% in VHDA, while the number hits 4.1 ± 0.1% in HDA. Since most of the interstitial molecules in VHDA are located at the pushed inward part of the normal second neighbor shell, whose distance from the central water molecule is larger than that in HDA, they have a less chance of hydrogen bonding to a central water molecule based on our definition. This corresponds to the previous consideration on PDOS figures of HDA and VHDA. This hypothesis has been confirmed in Figures 1 and 2 of ref 16, in which RDFs and the spatial distribution functions of HDA and VHDA have been given and HDA and VHDA indeed have distinct structures as described previously. In fact, we have carried out the same simulation for RDFs, and the same results of ref 16 were obtained.

With a larger occupancy of this interstitial location in VHDA, the locking up of the structure is likely to be greater than that of HDA, requiring additional kinetic energy to unlock it, namely, the VHDA−LDA transition temperature should be higher than the HDA−LDA transition temperature. However, the fraction of the interstitial molecules in HDA, which are hydrogen bonded to the central water molecules, is 4.1 ± 0.1%. This value is larger than the fraction of this kind of molecules of 2.8 ± 0.1% in VHDA. This difference induces more additional drops of potential of HDA than that of VHDA. The previous two influences compensate each other on the total energies of the two structures. Thus, the sum of both contributions on the total energies of the two structures leads to almost the same transition temperature of VHDA−LDA and HDA−LDA at ambient temperature, although it is known that the VHDA−LDA transition is measured at a heating rate of 10 K min^{-1}, while the HDA−LDA transition is determined at a very small heating rate.[17,18] Note that if the heating rate is considered, the HDA−LDA transition temperature is higher than the VHDA−LDA transition temperature or HDA is more stable than VHDA. This is true when the amorphous phases are at ambient pressure due to contributions of the hydrogen bonded interstitial molecules even if the interstitial molecule number in VHDA is almost double that in HDA.

Why are there some five hydrogen bonds water molecules in both HDA and VHDA but not in LDA? To form five hydrogen bonded water molecules, two conditions must be satisfied: (1) there must be at least one interstitial molecule and (2) the interstitial molecules and central water molecules must satisfy the geometric condition of hydrogen bond formation as we have defined previously, and they must have a connection with isosurfaces. Both HDA and VHDA satisfy the first condition, but LDA does not. To confirm the existence of five

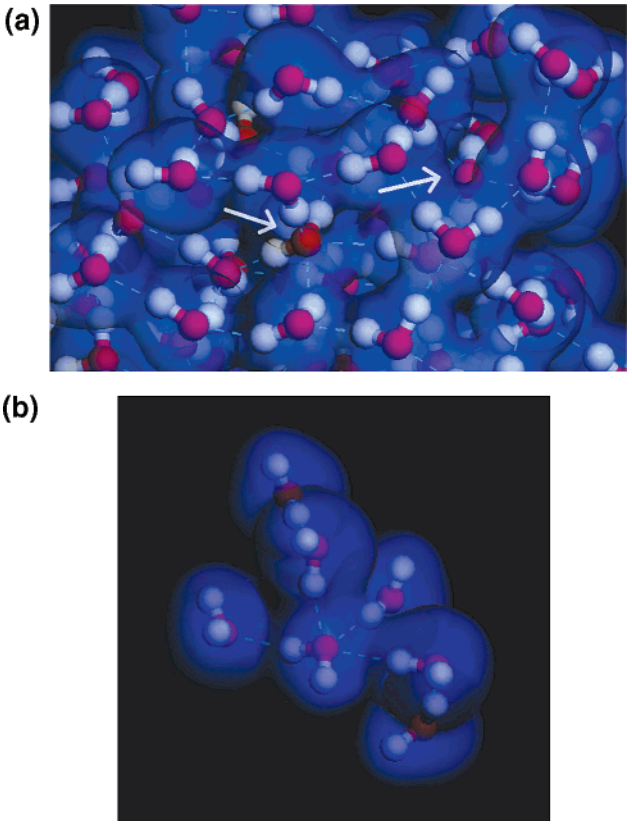

Figure 4. Isosurfaces of the charge density in 0.017 e/au^3 for (a) the regions of interest as discussed in the text indicated by arrows as well as (b) the interception of the arrow region in panel a where the fifth hydrogen bond shares lone electron pairs with the other two hydrogen bonds.

hydrogen bonded water molecules, or the satisfaction of the second condition, the electron densities of both HDA and VHDA are analyzed, as shown in Figure 4.

In Figure 4, the arrows indicate regions where the water molecules are bonded with five H ions, in which all five water molecules satisfy the hydrogen bond criteria. Pairs of water molecules that are identified as hydrogen bonded by the geometric definition share regions of high charge densities, and the molecules are surrounded by connected isosurfaces. In other words, three water molecules form hydrogen bonds with the O ion of central water molecules, and their isosurfaces all connect to the central water molecule and overlap each other. The fifth hydrogen bond shares lone electron pairs with the other two hydrogen bonds.

Conclusions

In summary, the structural and electronic properties of ice I*h*, HDA, and VHDA at $T = 77$ K under $P = 0.1$ MPa are determined, providing a detailed band structure, DOS, and PDOS of them. There are some five hydrogen bonded water molecules in both HDA ($4.1 \pm 0.1\%$) and VHDA ($2.8 \pm 0.1\%$) but not in the LDA, which are confirmed by PDOS analysis for these amorphous ices. Water molecules in VHDA have two interstitial neighbors and HDA have just one, whereas the fraction of interstitial molecules that are hydrogen bonded is somewhat larger in HDA ($4.1 \pm 0.1\%$) than in VHDA ($2.8 \pm 0.1\%$). This discrepancy is induced by that the nonbonded interstitial molecules in VHDA are more than that in HDA because they are located at a somewhat larger distance. As a result, HDA−LDA and VHDA−LDA transitions have almost the same transition temperature.

Acknowledgment. The authors acknowledge support by National Key Basic Research and Development Program (Grant 2004CB619301) and by Project 985-Automotive Engineering of Jilin University.

References and Notes

(1) Martonak, R.; Donadio, D.; Parrinello, M. *J. Chem. Phys.* **2005**, *122*, 134501.
(2) Saitta, M.; Strassle, T.; Rousse, G.; Hamel, G.; Klotz, S.; Nelmes, R. J.; Loveday, J. S. *J. Chem. Phys.* **2004**, *121*, 8430.
(3) Malcolm, G.; Chris, A. T.; Chris, J. B.; Dennis, D. K. *Chem. Phys. Lett.* **2004**, *397*, 335.
(4) Martonak, R.; Donadio, D.; Parrinello, M. *Phys. Rev. Lett.* **2004**, *92*, 225702.
(5) Starr, F. W.; Bellissent-Funel, M. C.; Stanley, H. E. *Phys. Rev. B* **1999**, *60*, 1084.
(6) Mishima, O.; Calvert, L. D.; Whalley, E. *Nature* **1984**, *310*, 393.
(7) Mishima, O.; Calvert, L. D.; Whalley, E. *Nature* **1985**, *314*, 76.
(8) Floriano, M. A.; Handa, Y. P.; Klug, D. D.; Whalley, E. *J. Chem. Phys.* **1989**, *91*, 7187.
(9) Whalley, E.; Klug, D. D.; Handa, Y. P. *Nature* **1989**, *342*, 782.
(10) Tse, J. S. *J. Chem. Phys.* **1992**, *96*, 5482.
(11) Tse, J. S.; Klug, D. D.; Tulk, C. A.; Swainson, I.; Svensson, E. C.; Loong, C. K.; Shpakov, V.; Belosludov, V. R.; Belosludov, R. V.; Kawazoe, Y. *Nature* **1999**, *400*, 647.
(12) Debenedetti, P. G. *Metastable Liquids*; Princeton University Press: Princeton, NJ, 1996.
(13) Mishima, O.; Stanley, H. E. *Nature* **1998**, *396*, 329.
(14) Kuhs, W. F.; Finney, J. L.; Vettier, C.; Bliss, D. V. *J. Chem. Phys.* **1984**, *81*, 3612.
(15) Finney, J. L.; Hallbrucker, A.; Kohl, I.; Soper, A. K.; Bowron, D. T. *Phys. Rev. Lett.* **2002**, *88*, 225503.
(16) Finney, J. L.; Bowron, D. T.; Soper, A. K.; Loerting, T.; Mayer, E.; Hallbrucker, A. *Phys. Rev. Lett.* **2002**, *89*, 205503.
(17) Tulk, C. A.; Benmore, C. J.; Urquidi, J.; Klug, D. D.; Neuefind, J.; Tomberli, B.; Egelstaff, P. A. *Science* **2002**, *297*, 1320.
(18) Koza, M. M.; Schober, H.; Fischer, H. E.; Hansen, T.; Fujara, F. *J. Phys.: Condens. Matter* **2003**, *15*, 321.
(19) Lynden-Bell, R. M.; Debenedetti, P. G. *J. Phys. Chem. B* **2005**, *109*, 6527.
(20) Nagy, P. I.; Erhardt, W. *J. Phys. Chem. B* **2005**, *109*, 5855.
(21) Starr, F. W.; Sciortino, F.; Stanley, H. E. *Phys. Rev. E* **1999**, *60*, 6757.
(22) Giovambattista, N.; Stanley, H. E.; Sciortino, F. *Phys. Rev. Lett.* **2003**, *91*, 115504.
(23) Chatterjee, A.; Ebina, T.; Mizukami, F. *J. Phys. Chem. B* **2005**, *109*, 7306.
(24) Simon, C.; Klein, M. L. *ChemPhysChem* **2005**, *6*, 148.
(25) Yamada, M.; Stanley, H. E.; Sciortino, F. *Phys. Rev. E* **2003**, *67*, 10202.
(26) Hale, B. N.; DiMattio, D. J. *J. Phys. Chem. B* **2004**, *108*, 19780.
(27) McBride, C.; Vega, C.; Sanz, E.; Abascal, J. L. F. *J. Chem. Phys.* **2004**, *121*, 11907.
(28) Payne, M. C.; Teter, M. P.; Allan, D. C.; Arias, T. A.; Joannopoulos, J. D. *Rev. Mod. Phys.* **1992**, *64*, 1045.
(29) Loerting, T.; Salzmann, C.; Kohl, I.; Mayer, E.; Hallbrucker, A. *Phys. Chem. Chem. Phys.* **2001**, *3*, 5355.
(30) Parrinello, M.; Rahman, A. *Phys. Rev. Lett.* **1980**, *45*, 1196.
(31) Berendsen, H. J. C.; Postma, J. P. M.; van Gunsteren, W. F.; DiNola, A.; Haak, J. R. *J. Chem. Phys.* **1984**, *81*, 3684.
(32) Essmann, U.; Perera, L.; Berkowitz, M. L.; Darden, T.; Lee, H.; Pedersen, L. G. *J. Chem. Phys.* **1995**, *103*, 8577.
(33) Mishima, O. *Nature* **1996**, *384*, 546.
(34) Bizid, A.; Bosio, L.; Defrain, A.; Oumezzine, M. *J. Chem. Phys.* **1987**, *87*, 2225.